





Electromechanical substrate characterization in arrhythmogenic cardiomyopathy using imaging-based patient-specific computer simulations

Nick van Osta ^{1,*†}, Feddo Kirkels^{1,2†}, Aurore Lyon ¹, Tijmen Koopsen¹, Tim van Loon¹, Maarten-Jan Cramer², Arco J. Teske², Tammo Delhaas ¹, and Joost Lumens ¹

¹Department of Biomedical Engineering, Cardiovascular Research Institute Maastricht, Maastricht University, Universiteitssingel 50 (UNS50), 6229 ER Maastricht, The Netherlands; and ²Division Heart and Lungs, Department of Cardiology, University Medical Center Utrecht, Utrecht, The Netherlands

Received 30 November 2020; editorial decision 5 December 2020; accepted after revision 14 December 2020

Aims

Arrhythmogenic cardiomyopathy (AC) is an inherited cardiac disease, characterized by life-threatening ventricular arrhythmias and progressive cardiac dysfunction. The aim of this study is to use computer simulations to non-invasively estimate the individual patient's myocardial tissue substrates underlying regional right ventricular (RV) deformation abnormalities in a cohort of AC mutation carriers.

Methods and results

In 68 AC mutation carriers and 20 control subjects, regional longitudinal deformation patterns of the RV free wall (RVfw), interventricular septum (IVS), and left ventricular free wall (LVfw) were obtained using speckle-tracking echocardiography. We developed and used a patient-specific parameter estimation protocol based on the multi-scale CircAdapt cardiovascular system model to create virtual AC subjects. Using the individual's deformation data as model input, this protocol automatically estimated regional RVfw and global IVS and LVfw tissue properties. The computational model was able to reproduce clinically measured regional deformation patterns for all subjects, with highly reproducible parameter estimations. Simulations revealed that regional RVfw heterogeneity of both contractile function and compliance were increased in subjects with clinically advanced disease compared to mutation carriers without clinically established disease ($17 \pm 13\%$ vs. $8 \pm 4\%$, $P = 0.01$ and $18 \pm 11\%$ vs. $10 \pm 7\%$, $P < 0.01$, respectively). No significant difference in activation delay was found.

Conclusion

Regional RV deformation abnormalities in AC mutation carriers were related to reduced regional contractile function and tissue compliance. In clinically advanced disease stages, a characteristic apex-to-base heterogeneity of tissue abnormalities was present in the majority of the subjects, with most pronounced disease in the basal region of the RVfw.

Keywords

Arrhythmogenic right ventricular cardiomyopathy • Computer modelling and simulation • Deformation imaging • Contractility • Right ventricle

* Corresponding author. E-mail address: n.vanosta@maastrichtuniversity.nl

† The first two authors contributed equally to the study.

© The Author(s) 2021. Published by Oxford University Press on behalf of the European Society of Cardiology.

This is an Open Access article distributed under the terms of the Creative Commons Attribution Non-Commercial License (<http://creativecommons.org/licenses/by-nc/4.0/>), which permits non-commercial re-use, distribution, and reproduction in any medium, provided the original work is properly cited. For commercial re-use, please contact journals.permissions@oup.com

What's new?

- We present a patient-specific modelling approach and show its ability to reproduce regional ventricular deformation patterns and to estimate the underlying tissue properties in arrhythmogenic cardiomyopathy (AC) mutation carriers.
- Patient-specific computer simulations reveal an increased heterogeneity in regional right ventricular (RV) contractility and compliance in clinically progressed disease stages.
- In most AC mutation carriers, myocardial disease is most progressed in the basal segment of the RVfw.

Introduction

Arrhythmogenic cardiomyopathy (AC) is an inherited heart muscle disorder characterized by fibrofatty replacement of primarily the right ventricular (RV) myocardium, which predisposes to ventricular arrhythmias and sudden cardiac death (SCD) in young individuals.^{1,2} Variable disease expression is found in familial AC,³ ranging from SCD in young individuals to a lifelong absence of any phenotype. To prevent apparently healthy AC mutation carriers from SCD, early detection of potentially pro-arrhythmic tissue substrates is important.

Using speckle-tracking echocardiography, our groups⁴ found distinct regional RV deformation abnormalities in AC mutation carriers. Predominantly the basal (subtricuspid) part of the RVfw was affected, even in the absence of electrocardiographic or structural 2010 Task Force Criteria (TFC).⁵ Using computer simulations, it was hypothesized that these deformation abnormalities resulted from a decreased contractility and an increased stiffness within this segment. In a follow-up study, these RV deformation abnormalities were found to be associated with AC disease progression.⁶ Another approach, as reported by Sarvari *et al.*⁷ showed that RV mechanical dispersion (RVMD), defined as the standard deviation in time-to-peak strain, is a marker for arrhythmic events in AC patients. The latter study demonstrate the prognostic value of RV longitudinal strain, while the disease substrates underlying the deformation abnormalities remain unknown. Together with the first study by Mast *et al.*,⁴ these studies suggest that identification of the disease substrate causing RV deformation abnormalities could be used to better understand disease progression and support risk stratification. Patient-specific characterization of the electromechanical disease substrates in early-stage AC may lead to better arrhythmic risk stratification and ultimately to the identification of possible therapeutic targets, thereby enabling personalized medicine. Since invasive tissue characterization is accompanied by important risks, and is rarely performed, non-invasive ways of tissue characterization should be investigated.

The aim of this study is to non-invasively estimate the pathophysiological substrates underlying regional deformation abnormalities in the individual AC mutation carrier, using imaging-based patient-specific computer simulations. We use a parameter estimation protocol based on a previously established framework⁸ which simulates myocardial deformation to identify regional tissue properties.

Methods

Patient cohort

This study was performed on a previously reported consecutive cohort of pathogenic desmosomal mutation carriers, who were evaluated at the UMC Utrecht in the Netherlands between 2006 and 2015.⁴ During this period, 87 subjects carrying a pathogenic plakophilin-2 (PKP2), desmoglein-2 (DSG2), or desmoplakin (DSP) mutation were evaluated. Additionally, 20 healthy volunteers were included as control subjects. The study was approved by the local institutional ethics review board.

The echocardiographic protocol has been detailed elsewhere.⁹ Briefly, all echocardiographic data were obtained on a Vivid 7 or Vivid E9 ultrasound machine (GE Vingmed Ultrasound, Horten, Norway) using a broadband M3S transducer and were analysed for fulfilling 2010 TFC for structural abnormalities.⁵ Only exams during sinus rhythm were eligible for inclusion. Conventional two-, three-, and four-chamber views, as well as an RV-focused apical four-chamber view, were used to visualize the RV lateral free wall (RVfw), interventricular septum (IVS), and left ventricular (LV) free wall (LVfw). Cine-loops were stored for offline two-dimensional speckle tracking using EchoPAC v. 202 (GE Vingmed Ultrasound, Horten, Norway). A single observer, blinded to clinical information, obtained segmental longitudinal strain curves of the RVfw and the left ventricle.

In this study, we focused on regional heterogeneity of RVfw tissue abnormalities because the RVfw is the most affected area in pathogenic desmosomal mutation carriers.¹⁰ Therefore, three segmental deformation patterns of the RVfw (i.e. apical, mid-ventricular and basal) were used to personalize the computational model (Figure 1). Additionally, two global deformation patterns of the LVfw and IVS were used to ensure realistic mechanical boundary conditions for the RVfw in terms of ventricular interaction. Global LVfw and IVS deformation patterns were obtained by averaging the 12 LVfw and 6 IVS segmental deformation curves, respectively, using the standardized 18-segment model.¹¹

Cardiac magnetic resonance imaging (CMR) was performed on a 1.5-T scanner (Achieva, Philips Healthcare, Best, the Netherlands), according to standard AC protocols,¹² and included measurements of the RV end-diastolic volume, RV ejection fraction, and LV ejection fraction. LV stroke volume was used to personalize cardiac output (CO) in the computer simulations.

For further analysis, RV disease substrates were categorized by three different non-invasive imaging approaches, which have been published previously:

- (1) following the revised 2010 TFC,⁵ AC can be divided into three consecutive clinical stages: (i) subclinical (concealed) stage with absence of any 2010 TFC, except for harbouring a pathogenic mutation; (ii) electrical stage, with only electrocardiographic (ECG) or Holter abnormalities; and (iii) structural stage, with structural abnormalities on non-invasive imaging, regardless of the history of ventricular arrhythmias or presence of ECG or Holter abnormalities.^{5,13}
- (2) based on the pattern of basal RVfw deformation following the pre-defined criteria published by Mast *et al.*⁴ A Type I pattern is defined as normal deformation; a Type II pattern is characterized by delayed onset of shortening, reduced systolic peak strain and minor post-systolic shortening; a Type III pattern is characterized by little or no systolic peak strain, predominantly systolic stretching and major post-systolic shortening;
- (3) based on RVMD, an index of segmental heterogeneity in contraction in the RVfw and IVS. RVMD was calculated on six segments of the right ventricle, including the IVS, and defined as the standard deviation of the segmental time intervals from onset Q/R on the

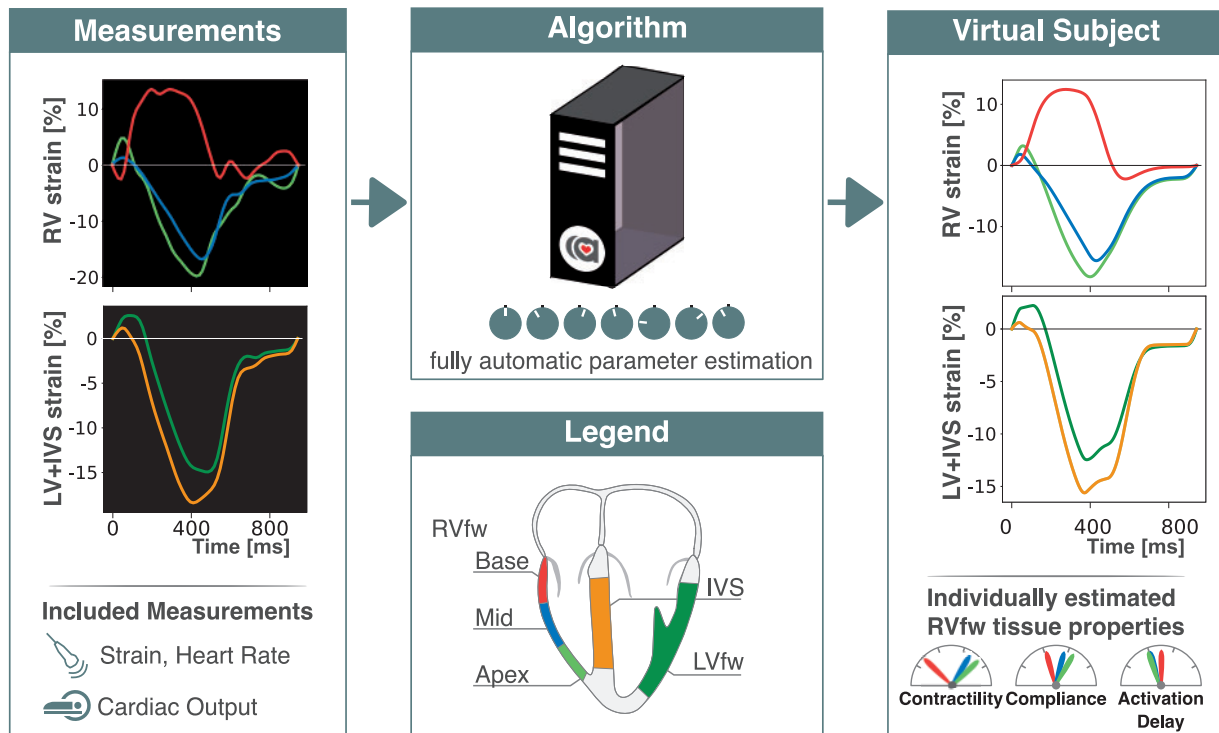


Figure 1 Methodology. Right ventricular (RV), interventricular septal (IVS), and left ventricular (LV) strain were obtained using speckle-tracking echocardiography, and cardiac output was obtained using cardiovascular magnetic resonance imaging (CMR). Using a fully automatic estimation protocol, virtual subjects reproducing the clinical measures were generated and local tissue properties were extracted.

surface ECG to peak negative strain.⁷ A previously established cut-off value of 30 ms¹⁴ was used in this study to define a group with low and high RVMD.

Computer simulations

Regional RV, IVS, and LV myocardial deformation were simulated using the CircAdapt model,¹⁵ which is a closed-loop lumped parameter computer model of the human heart and circulation. It enables simulation of cardiac haemodynamics and regional wall mechanics, using a phenomenological model describing active and passive myofibre mechanics.¹⁶ Ventricular interactions are modelled using the TriSeg model using the concept of conservation of energy.¹⁷ LVfw and IVS were modelled as a single segment representing the mechanics of the entire wall. Three RVfw segments representing the apical, mid-ventricular, and basal regions were modelled using the previously validated MultiPatch model.¹⁶

Patient-specific simulation protocol

Computer simulations were personalized by automatically tuning model parameters to optimize the modelled myofibre strain to measured longitudinal strain (Figure 1). A parameter subset with 21 parameters essential for modelling regional RVfw, IVS, and LVfw deformation in AC mutation carriers was previously identified.⁸ CO and heart rate (HR) were direct input parameters of the model and thereby set from the measurements. The former was obtained from CMR data, while the latter was obtained from the RV focused four-chamber view. The other 19 parameters describe the size of the RVfw, IVS, and LVfw (three model parameters), myocardial twitch duration and thus relative systolic duration (one

parameter), and three regional tissue properties per myocardial segment being contractility, compliance, and activation delay (i.e. 15 model parameters in total).

Parameters were individually estimated using a parameter estimation framework previously described in more detail.⁸ This framework estimates model parameters using the clinical data as described above and results in a virtual subject that reproduces the clinical data. In brief, the parameter estimation framework consisted of two steps. First, with CO and HR set to the measured values, 5000 quasi-random Monte Carlo simulations were performed from which the best 60 simulations were used as initial candidate solutions. Second, these candidate simulations were optimized using the stochastic multi-swarm particle swarm optimization (MSPSO).^{18,19} MSPSO is an evolutionary algorithm, where a population of candidate solutions moves through the input space driven by their history and the history of a changing subpopulation. A more detailed description of the methodology used is provided in the [Supplementary material online](#). Eventually, this parameter estimation protocol results in a virtual patient, from which regional tissue properties can be extracted.

Local tissue properties

RVfw contractility, compliance, and activation delay were extracted from the resulting virtual patient simulations and the heterogeneity of these tissue properties was investigated. Due to the nonlinearity, non-monotonicity, and non-additivity of the lumped system, the individual estimated parameters were not interpreted directly, but local tissue properties were derived from the simulated time signals of myofibre stress and strain. As the RVfw is typically most affected in desmosomal mutation

carriers,¹ we focus on the heterogeneity in regional RVfw tissue properties. To limit the degrees of freedom in the model, parameters in the left ventricle and IVS were not estimated on a segmented level, but in a single segment representing the entire wall to include ventricular interaction.

The exact methodology used to quantify regional myocardial contractility, compliance, and activation delay was described in more detail in the [Supplementary material online](#). In brief, segmental contractility was defined as the maximum rate of active stress rise, which can be seen as the equivalent of the maximum rate of ventricular systolic pressure rise (dP/dt_{\max}) on a local tissue level. Segmental wall compliance was defined as the slope of the end-diastolic myofibre stress-strain relationship, obtained using a preload manipulation. This is the regional equivalent of the slope of the global end-diastolic pressure–volume relation. Furthermore, regional activation delay was defined as the time delay of onset active stress development relative to the first activated segment.

Reproducibility

To determine reproducibility, a separate validation set was used. Two separate observers blinded to clinical data performed deformation analysis twice in nine subjects with a pathogenic desmosomal mutation, resulting in four different deformation datasets per patient. Each dataset was used three times as input for the parameter estimation framework described above. Inter- and intra-observer agreement, as well as the uniqueness of parameter estimation were determined using the intraclass correlation coefficient (ICC).²⁰ This protocol is explained in more detail in the [Supplementary material online](#).

Statistical analysis

Continuous data were presented as mean \pm standard deviation. Normal distribution was tested using the Shapiro–Wilk test. Comparison between subgroups of continuous variables was done using a one-way analysis of variance, *t*-test, Kruskal–Wallis, or Mann–Whitney *U* test as appropriate. Bonferroni correction was used to adjust for multiple comparisons. All statistical analyses were performed in Python 3.6.4 using the packages SciPy (modified BSD License) and statsmodels (modified BSD License).

Results

From the 87 AC mutation carriers who were evaluated, 3 subjects were excluded due to inadequate echocardiographic imaging quality and 16 were excluded due to missing CMR data. All remaining exams were obtained during sinus rhythm. The 68 AC mutation carriers included in this study (18 probands and 50 family members) had a mean age of 39 ± 17 years and 41 (60%) were female. Among the different pathogenic mutations, PKP2 was most common in this cohort (90%). A total of 20 control subjects [9 (45%) females, mean age 28 ± 6 years] were also included in the study. Using the 2010 TFC, 18 (26%) mutation carriers were classified in the subclinical stage, 15 (22%) in the electrical stage, and 35 (51%) in the structural stage. The median time between echocardiography and CMR was 26 days [interquartile range (–7, 398 days)] ([Table 1](#)).

Typical examples of measured and simulated ventricular deformation curves in a control subject and subjects in the subclinical, electrical, and structural AC disease stages are shown in [Figure 2](#). Most healthy controls ($n = 20$, 100%) and subclinical stage subjects ($n = 12$, 67%) had a Type I deformation pattern and thus showed relatively

homogeneous deformation patterns in the three RVfw segments. However, 6 (33%) subclinical subjects had an abnormal Type II deformation pattern in the RVfw basal segment. Most subjects in the electrical stage showed heterogeneous deformation patterns with predominantly basal abnormalities [Type II: $n = 8$ (53%) and Type III: $n = 3$ (20%)], which were even more severe in the structural stage subjects [Type II: $n = 10$ (29%) and Type III: $n = 23$ (66%)].

Contractility

Overall, heterogeneity in regional RVfw contractility was higher in the electrical and structural stage groups compared to the subclinical stage and control groups (control: $9.98 \pm 4.27\%$; subclinical: $7.57 \pm 4.47\%$; electrical: $17.23 \pm 15.92\%$; structural: $16.94 \pm 13.28\%$, $P = 0.011$). In general, the basal contractility was lower compared to the apical contractility ([Figure 3](#)). A few individuals ($n = 9$, 13%), however, were found to have lower apical than basal contractility. No significant difference was found in average RVfw contractility (control: 363 ± 175 kPa/s; subclinical: 373 ± 131 kPa/s; electrical: 421 ± 167 kPa/s; structural: 442 ± 174 kPa/s) ($P = 0.470$).

Compliance

Heterogeneity in regional RVfw compliance was increased in the electrical and structural stage groups compared to the subclinical stage and control groups (control: $9.16 \pm 4.84\%$; subclinical: $10.46 \pm 7.11\%$; electrical: $12.49 \pm 9.63\%$; structural: $18.45 \pm 11.00\%$, $P = 0.002$). On average, compliance was lower in the basal segment compared to the apical segment ([Figure 3](#)). Average RVfw compliance was not significantly different between the groups (control: $500 \pm 325\%/kPa$; subclinical: $551 \pm 561\%/kPa$; electrical: $1002 \pm 723\%/kPa$; structural: $742 \pm 595\%/kPa$, $P = 0.094$).

Activation delay

No significant difference was found in heterogeneity of regional RVfw activation delay (control: 10 ± 11 ms; subclinical: 8.9 ± 10.1 ms; electrical: 21 ± 30 ms; structural: 18 ± 22 ms, $P = 0.267$). However, the electrical and structural stage groups contained more individuals with a relatively late activated basal segment than the subclinical stage and control groups.

Basal deformation patterns

The simulations revealed that heterogeneity in RVfw contractility was increased in compared to the Type I and control groups (control: $9.98 \pm 4.27\%$; Type I: $6.52 \pm 5.20\%$; Type II: $12.19 \pm 11.25\%$; Type III: $21.81 \pm 14.09\%$, $P < 0.001$). Also, the heterogeneity in compliance was increased in the groups with Type II and Type III RV basal deformation patterns compared to the Type I and control groups (control: $9.16 \pm 4.84\%$; Type I: $9.43 \pm 5.78\%$; Type II: $13.00 \pm 8.46\%$; Type III: $20.63 \pm 11.74\%$, $P < 0.001$). No significant difference was found in activation delay (control: 10.0 ± 11.1 ms; Type I: 8.4 ± 6.3 ms; Type II: 16.6 ± 25.5 ms; Type III: 21.3 ± 24.7 ms, $P = 0.472$).

Right ventricular mechanical dispersion

Increased RVMD in pathogenic desmosomal mutation carriers was only related to increased heterogeneity in contractility ($20.0 \pm 14.7\%$) compared to the group with normal RVMD ($7.70 \pm 4.99\%$)

Table 1 Clinical characteristics

	Controls (n = 20)	Subclinical stage (n = 18)	Electrical stage (n = 15)	Structural stage (n = 35)	
Age (years)	28 ± 6	27 ± 14	40 ± 17 [§]	44 ± 16	P < 0.001
Female	9 (45%)	11 (61%)	12 (80%)	18 (51%)	
BSA (m ²)	1.87 ± 0.17	1.80 ± 0.21	1.84 ± 0.17	1.91 ± 0.22	P = 0.280
Probands	0 (0%)	0 (0%)	0 (0%)	18 (53%)	
AC diagnosis	0 (0%)	0 (0%)	5 (33%)	35 (100%)	
2010 TFC (major or minor)					
Structural criteria		0 (0%)	0 (0%)	35 (100%)	
Depolarization criteria		1 (6%)	12 (80%)	17 (49%)	
Repolarization criteria		1 (6%)	3 (20%)	20 (57%)	
Arrhythmia criteria		0 (0%)	5 (33%)	32 (91%)	
Mutations					
PKP2 mutation		15 (83%)	14 (93%)	32 (91%)	
DSG2 mutation		3 (17%)	1 (7%)	2 (6%)	
DSP mutation		0 (0%)	0 (0%)	1 (3%)	
CMR					
CO (L/min/m ²)	3.7 ± 0.6	3.3 ± 0.5	3.5 ± 0.6	3.2 ± 0.8	P = 0.041
RV-EDVi (mL/m ²)	108 ± 17	87 ± 17	94 ± 12	132 ± 41*	P < 0.01
LV-EDVi (mL/m ²)	98 ± 14	85 ± 13	93 ± 14	91.8 ± 15	P = 0.063
RVEF (%)	54 ± 6	56 ± 8	51 ± 6	36 ± 11*	P < 0.001
LVEF (%)	61 ± 7	58 ± 4	57 ± 7	56 ± 9	P = 0.182
Presence of LGE	0 (0%)	0 (0%)	0 (0%)	20 (57%)	
Echocardiography					
HR	62 ± 10	67 ± 16	63 ± 11	58 ± 9	P = 0.088
LV-GLS (%)	-21.1 ± 1.7	-20.0 ± 1.7	-19.0 ± 3.0	-17.8 ± 3.3*	P < 0.001
LVEF (%)	60.6 ± 6.9	58.4 ± 4.3	56.6 ± 6.8	55.8 ± 9.2	P = 0.159
RV-GLS (%)	-27.6 ± 4.0	-25.4 ± 3.6	-21.7 ± 4.7 [§]	-15.0 ± 5.6*	P < 0.001
RV basal deformation pattern					
Type I	20 (100%)	12 (67%)	4 (27%)	2 (6%)	
Type II	0 (0%)	6 (33%)	8 (53%)	10 (29%)	
Type III	0 (0%)	0 (0%)	3 (20%)	23 (66%)	
RVMD (ms)	—	16.4 ± 7.5	32.2 ± 16.1	50 ± 27	P < 0.01

AC, arrhythmogenic cardiomyopathy; CMR, cardiovascular magnetic resonance imaging; CO, cardiac output; DSG2, desmoglobin-2; DSP, desmoplakin; EDVi, end-diastolic volume indexed for BSA; GLS, global longitudinal strain; HR, heart rate; LGE, late gadolinium enhancement; LV, left ventricle; LVEF, left ventricular ejection fraction; PKP2, plakophilin-2; RV, right ventricle; RVEF, right ventricular ejection fraction; RVMD, right ventricular mechanical dispersion; TFC, Task Force Criteria.

*P < 0.05 structural stage vs. all other groups (Bonferroni correction).

†P < 0.05 structural stage vs. control group and subclinical stage.

§P < 0.05 electrical stage vs. control.

(P < 0.001). Regional heterogeneities of both compliance and activation delay were not significantly different between subjects with low and high RVMD (compliance: 16.0 ± 10.5% vs. 13.8 ± 10.2%, P = 0.054; activation delay: 20.6 ± 26.0 ms vs. 11.1 ± 15.6 ms, P = 0.195).

Parameter estimation

The estimated RV tissue properties were highly reproducible, with a minimum inter- and intra-observer ICC of 0.91 and 0.86, respectively. Reproducibility of the simulations was sufficient, with a minimum ICC of 0.76. In all simulations of the same subject, the trend in local RVfw heterogeneity was similar. More detailed reproducibility results can be found in the [Supplementary material online](#).

Discussion

In this study, patient-specific simulations were successfully used to estimate regional RVfw tissue properties from echocardiographic deformation imaging data in 68 subjects with a pathogenic AC mutation and 20 control subjects. Regional heterogeneities of contractility and compliance in the RVfw were largest in subjects in the structural disease stage. Our patient-specific simulations suggested that structural abnormalities according to the 2010 TFC were associated with an increased heterogeneity in RVfw myocardial tissue contractility and compliance. The most advanced disease substrates were found predominantly in the RVfw basal segment. To our knowledge, this is the first time that regional ventricular tissue properties are quantified using patient-specific simulations based on non-invasively measured

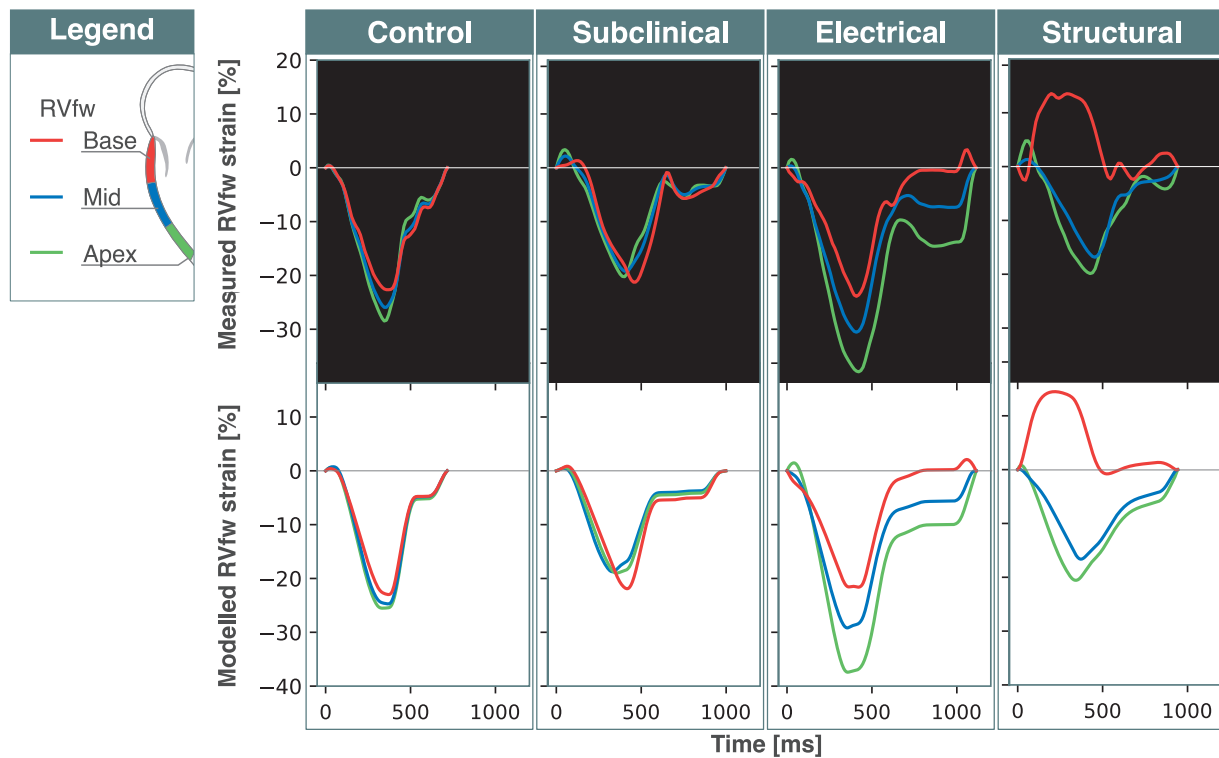


Figure 2 Typical regional right ventricular free wall (RVfw) strain patterns. Control subjects and most subjects in subclinical stage showed homogeneous strain patterns. Most subjects in the electrical and structural stage showed abnormal heterogeneous strain patterns.

longitudinal strain patterns. This method reveals potentially important information about myocardial disease substrates and thereby paves the way for personalized medicine.

In a previous study, we showed that desmosomal mutation carriers with more advanced AC disease stages have the most abnormal RV basal deformation pattern.⁴ In the same study, using computer simulations it was concluded that this abnormal mechanical behaviour of the right ventricle cannot be explained by an electromechanical activation delay alone. Non-personalized simulations representing subgroups of AC mutation carriers showed that at least some degree of local mechanical dysfunction was needed to reproduce the measured RV deformation abnormalities. A recently published sensitivity analysis⁸ confirmed that model parameters related to both activation delay and mechanical dysfunction are essential to reproduce myocardial deformation using the CircAdapt model.⁸ The current study extends this previous work by estimating patient-specific myocardial substrates in all three RVfw segments and by including the LV mechanics for a more realistic approach of the patient's haemodynamics. These patient-specific simulations confirmed hypothesis that abnormal deformation patterns are related to increased regional heterogeneity in contractility and compliance without a heterogeneity in activation delay.⁴

AC mutation carriers classified with structural abnormalities according to the 2010 TFC, being wall motion abnormalities such as akinesia, dyskinesia, or aneurysm in combination with RV dilatation or impaired RV systolic function measured by either CMR or echocardiography.⁵ These structural abnormalities result from fibrofatty

replacements of the RV myocardium, which affects regional wall motion and eventually global RV systolic function.² Also our computer simulations revealed the largest heterogeneity of RVfw tissue properties in the patients with structural stage disease, with the basal region of the RVfw being most affected by the disease. The few structural stage subjects with a relatively low heterogeneity of RV tissue properties showed highly impaired RV deformation with decreased contractility and compliance in all three segments, suggesting highly advanced AC disease.

Our patient-specific simulations suggested that the RV apex-to-base heterogeneity of mechanical behaviour in the more advanced AC disease stages is mostly due to decreased basal contractility and compliance. Several potential causes for AC-related changes in active and passive myocardial tissue properties have been identified in clinical and pre-clinical studies. One is the fibrofatty replacement of the myocardium,² which results in loss of contractile function and a change in passive tissue behaviour. Besides, Cerrone et al.²¹ found altered calcium transients in mice with a loss of PKP2 expression, including an increased calcium transient with an increased time-to-peak and a slower decay, suggesting a change in contractile function. To identify the exact (sub)cellular mechanisms underlying the regional RV deformation abnormalities in AC subjects beyond changes of tissue contractility and compliance, a more complex model of the myocardial electromechanics is needed.

In previous clinical studies, RVMD was associated with arrhythmic outcome.⁷ In our modelling study, a higher RVMD was associated with an increased heterogeneity of contractility in the RVfw, but not

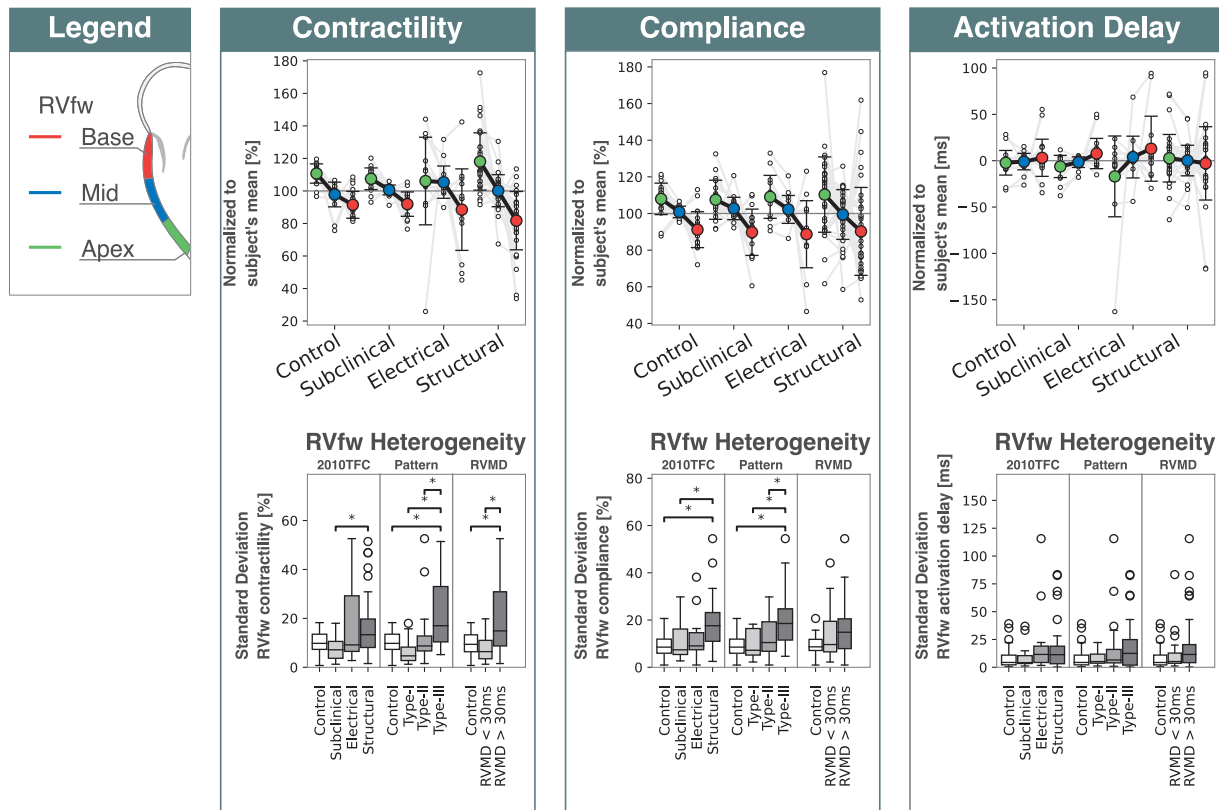


Figure 3 Estimated tissue properties. In the top row, RV regional estimations of contractility, compliance, and activation delay are shown relative to the mean value. In the bottom row, the standard deviation of these three properties is shown in a boxplot, characterized by 2010 TFC (subclinical, electrical, structural), strain morphology (Type I, Type II, and Type III), and RV mechanical dispersion (RVMD). * indicates a significant difference with $P < 0.05$.

with myocardial compliance. These contractile abnormalities could reflect calcium handling abnormalities, which form a possible pro-arrhythmic substrate. Interestingly, using the classification defined by Mast *et al.*,⁴ an abnormal Type III deformation pattern was reproduced by both abnormal contractility and abnormal compliance. Where RVMD is based only on timing of the longitudinal strain, the pattern classification is based on information of both timing and amplitude. Our computer simulations suggest that both classifications can detect a different kind of tissue substrate.

An RVfw apex-to-base heterogeneity was already present in the deformation measurements of healthy controls, resulting in heterogeneity in estimated tissue properties. Some level of 'physiological' heterogeneity in deformation is to be expected, since regional differences of ventricular tissue properties, such as activation delay,²² action potential morphology,²³ and wall thickness,²⁴ also exist in healthy hearts. Because the control group and subclinical group have a similar heterogeneity in tissue properties, it can be assumed that the observed heterogeneity in regional RV tissue properties is not abnormal.

Study limitations

Estimations are based on the average CO obtained from CMR and on regional LV and RV strain obtained from speckle tracking

echocardiography. CMR volumes were used because they provided the most reliable non-invasive estimation of CO and ventricular volumes. Because the CMR and the echocardiographic examination cannot be performed simultaneously, there is a potential mismatch between the two measurements. This mismatch might result in global under- or overestimation of ventricular tissue properties but is not expected to have a significant effect on the heterogeneity in RVfw tissue properties.

The deformation measurements were obtained from four different heartbeats. We did not correct for any measurement errors, such as timing errors between the four echo views, beat-to-beat variability, or respiration. Future studies could investigate how to design an objective function using strain indices or other measurements, such as valve timings, blood flow velocity or ejection fraction, to develop a more efficient fitting algorithm with an objective function invariant of measurement uncertainties.

Future work

A longitudinal study, in which follow-up data is included, should be performed to reveal whether and how this disease substrate progresses in individuals, and whether any kind of disease evolution could be used for prediction of arrhythmic outcome in a clinical setting.

The majority of this retrospective study cohort consisted of PKP2 mutation carriers. Future prospective verification studies are needed to confirm our findings and to determine whether our results can be extrapolated to AC patients with a different genetic background. The CircAdapt model is not limited to modelling AC disease substrates, so future work could also explore to which extent this framework is applicable to identify disease substrates in other cardiac pathologies.

Conclusion

We presented a patient-specific modelling approach and showed its ability to reproduce regional ventricular deformation patterns and to estimate the underlying tissue properties in AC mutation carriers. Patient-specific simulations revealed that regional RV deformation abnormalities were related to reduced contractile function and tissue compliance. In most subjects, a characteristic apex-to-base heterogeneity of tissue abnormalities was present, whereby the basal region of the RVfw was most affected. Tissue abnormalities were most pronounced in the subjects with a clinically more advanced disease stage. Future studies should investigate whether simulation-based characterization of patient-specific disease substrates can be used for personalized prediction of AC disease progression or arrhythmic events.

Supplementary material

Supplementary material is available at *Europace* online.

Funding

This work was supported by the Netherlands Organisation for Scientific Research (NWO-ZonMw, VIDI grant 016.176.340 to J.L.) and the Dutch Heart Foundation (ERA-CVD JTC2018 grant 2018T094; Dr Dekker Program grant 2015T082 to J.L.). The funders had no role in study design or data acquisition. This paper is part of a supplement supported by an unrestricted grant from the Theo-Rossi di Montelera (TRM) foundation.

Conflict of interest: none declared.

Data availability

The source code supporting this article has been uploaded as part of the electronic [supplementary material](#).

References

1. Thiene G, Nava A, Corrado D, Rossi L, Pennelli N. Right ventricular cardiomyopathy and sudden death in young people. *N Engl J Med* 1988;**318**:129–33.
2. Basso C, Corrado D, Marcus FI, Nava A, Thiene G. Arrhythmogenic right ventricular cardiomyopathy. *Lancet* 2009;**373**:1289–300.
3. Groeneweg JA, Bhonsale A, James CA, Riele AS, Te Dooijes D, Tichnell C et al. Clinical presentation, long-term follow-up, and outcomes of 1001 arrhythmogenic right ventricular dysplasia/cardiomyopathy patients and family members. *Circ Cardiovasc Genet* 2015;**8**:437–46.
4. Mast TP, Teske AJ, Walmsley J, Heijden JF, van der Es R, van Prinzen FW et al. Right ventricular imaging and computer simulation for electromechanical substrate characterization in arrhythmogenic right ventricular cardiomyopathy. *J Am Coll Cardiol* 2016;**68**:2185–97.
5. Marcus FI, McKenna WJ, Sherrill D, Basso C, Bauce B, Bluemke DA et al. Diagnosis of arrhythmogenic right ventricular cardiomyopathy/dysplasia: proposed modification of the task force criteria. *Eur Heart J* 2010;**31**:806–14.
6. Mast TP, Taha K, Cramer MJ, Lumens J, Heijden JF, van der Bouma BJ et al. The prognostic value of right ventricular deformation imaging in early arrhythmogenic right ventricular cardiomyopathy. *JACC Cardiovasc Imaging* 2019;**12**:446–55.
7. Sarvari SI, Haugaa KH, Anfinson OG, Leren TP, Smiseth OA, Kongsgaard E et al. Right ventricular mechanical dispersion is related to malignant arrhythmias: a study of patients with arrhythmogenic right ventricular cardiomyopathy and sub-clinical right ventricular dysfunction. *Eur Heart J* 2011;**32**:1089–96.
8. van ON, Lyon A, Kirkels F, Koopsen T, van LT, Cramer MJ et al. Parameter subset reduction for patient-specific modelling of arrhythmogenic cardiomyopathy-related mutation carriers in the CircAdapt model. *Philos Trans A Math Phys Eng Sci* 2020;**378**:20190347.
9. Teske AJ, Bw De B, Melman PG, Sieswerda GT, Doevendans PA, Cramer MJ. Echocardiographic quantification of myocardial function using tissue deformation imaging, a guide to image acquisition and analysis using tissue Doppler and speckle tracking. *Cardiovasc. Ultrasound* 2007;**5**:27.
10. Te Riele ASJM, James CA, Philips BINU, Rastegar NEDA, Bhonsale A, Groeneweg JA et al. Mutation-positive arrhythmogenic right ventricular dysplasia/cardiomyopathy: the triangle of dysplasia displaced. *J Cardiovasc Electrophysiol* 2013;**24**:1311–20.
11. Voigt JU, Pedrizzetti G, Lysyansky P, Marwick TH, Houle H, Baumann R et al. Definitions for a common standard for 2D speckle tracking echocardiography: consensus document of the EACVI/ASE/Industry Task Force to standardize deformation imaging. *Eur Heart J Cardiovasc Imaging* 2015;**16**:1–11.
12. Dalal D, Tandri H, Judge DP, Amat N, Macedo R, Jain R et al. Morphologic variants of familial arrhythmogenic right ventricular dysplasia/cardiomyopathy: a genetics–magnetic resonance imaging correlation study. *J Am Coll Cardiol* 2009;**53**:1289–99.
13. Te Riele ASJM, James CA, Rastegar N, Bhonsale A, Murray B, Tichnell C et al. Yield of serial evaluation in at-risk family members of patients with ARVD/C. *J Am Coll Cardiol* 2014;**64**:293–301.
14. Haugaa KH, Basso C, Badano LP, Bucciarelli-Ducci C, Cardim N, Gaemperli O et al.; EACVI Scientific Documents Committee, EACVI Board members and external reviewers. Comprehensive multi-modality imaging approach in arrhythmogenic cardiomyopathy—an expert consensus document of the European Association of Cardiovascular Imaging. *Eur Heart J Cardiovasc Imaging* 2017;**18**:237–53.
15. Arts T, Delhaas T, Bovendeerd P, Verbeek X, Prinzen F. Adaptation to mechanical load determines shape and properties of heart and circulation: the CircAdapt model. *Am J Physiol Heart Circ Physiol* 2005;**288**:1943–54.
16. Walmsley J, Arts T, Derval N, Bordachar P, Cochet H, Ploux S et al. Fast simulation of mechanical heterogeneity in the electrically asynchronous heart using the MultiPatch module. *PLoS Comput Biol* 2015;**11**:1–23.
17. Lumens J, Delhaas T, Kim B, Arts T. Three-wall segment (TriSeg) model describing mechanics and hemodynamics of ventricular interaction. *Ann Biomed Eng* 2009;**37**:2234–55.
18. Kennedy J, Eberhart R. Particle swarm optimization. Proceedings of ICNN'95 - International Conference on Neural Networks IEEE November 1995;**4**:1942–8.
19. Liang JJ, Suganthan PN. Dynamic multi-swarm particle swarm optimizer. In: Proc - 2005 IEEE Swarm Intell Symp SIS 2005; IEEE, 2005:124–9.
20. Koo TK, Li MY. A guideline of selecting and reporting intraclass correlation coefficients for reliability research. *J Chiropr Med* 2016;**15**:155–63.
21. Cerrone M, Montnach J, Lin X, Zhao YT, Zhang M, Agullo-Pascual E et al. Plakophilin-2 is required for transcription of genes that control calcium cycling and cardiac rhythm. *Nat Commun* 2017;**8**:106.
22. Durrer D, Dam Rt van, Freud GE, Mj J, Meijler FL, Arzbaecher RC. Total excitation of the isolated human heart. *Circulation* 1970;**41**:899–912.
23. Antzelevitch C, Fish J. Electrical heterogeneity within the ventricular wall. *Basic Res Cardiol* 2001;**96**:517–27.
24. Kawel-Boehm N, Maceira A, Valsangiacomo-Buechel ER, Vogel-Claussen J, Turkbey EB, Williams R et al. Normal values for cardiovascular magnetic resonance in adults and children. *J Cardiovasc Magn Reson* 2015;**17**:33.